

Dear Author,

Here are the proofs of your article.

- You can submit your corrections **online** or by **fax**.
- For **online** submission please insert your corrections in the online correction form. Always indicate the line number to which the correction refers.
- Please return your proof together with the **permission to publish** confirmation.
- For **fax** submission, please ensure that your corrections are clearly legible. Use a fine black pen and write the correction in the margin, not too close to the edge of the page.
- Remember to note the journal title, article number, and your name when sending your response via e-mail, fax or regular mail.
- **Check** the metadata sheet to make sure that the header information, especially author names and the corresponding affiliations are correctly shown.
- **Check** the questions that may have arisen during copy editing and insert your answers/ corrections.
- **Check** that the text is complete and that all figures, tables and their legends are included. Also check the accuracy of special characters, equations, and electronic supplementary material if applicable. If necessary refer to the *Edited manuscript*.
- The publication of inaccurate data such as dosages and units can have serious consequences. Please take particular care that all such details are correct.
- Please **do not** make changes that involve only matters of style. We have generally introduced forms that follow the journal's style. Substantial changes in content, e.g., new results, corrected values, title and authorship are not allowed without the approval of the responsible editor. In such a case, please contact the Editorial Office and return his/her consent together with the proof.
- If we do not receive your corrections **within 48 hours**, we will send you a reminder.

Please note

Your article will be published **Online First** approximately one week after receipt of your corrected proofs. This is the **official first publication** citable with the DOI. **Further changes are, therefore, not possible.**

After online publication, subscribers (personal/institutional) to this journal will have access to the complete article via the DOI using the URL: [http://dx.doi.org/\[DOI\]](http://dx.doi.org/[DOI]).

If you would like to know when your article has been published online, take advantage of our free alert service. For registration and further information go to: www.springerlink.com.

Due to the electronic nature of the procedure, the manuscript and the original figures will only be returned to you on special request. When you return your corrections, please inform us, if you would like to have these documents returned.

The **printed version** will follow in a forthcoming issue.

Fax to: +44 870 622 1325 (UK) or +44 870 762 8807 (UK)



To: Springer Correction Team

6&7, 5th Street, Radhakrishnan Salai, Chennai, Tamil Nadu, India – 600004

Re: Computational Mechanics DOI:10.1007/s00466-009-0365-8

Torsional rigidity of a circular bar with multiple circular inclusions using the null-field integral approach

Authors: Jeng-Tzong Chen · Ying-Te Lee

Permission to publish

I have checked the proofs of my article and

- I have no corrections. The article is ready to be published without changes.
- I have a few corrections. I am enclosing the following pages:
- I have made many corrections. Enclosed is the complete article.

Date / signature _____

Metadata of the article that will be visualized in OnlineFirst

Please note: Images will appear in color online but will be printed in black and white.

ArticleTitle	Torsional rigidity of a circular bar with multiple circular inclusions using the null-field integral approach	
Article Sub-Title		
Article CopyRight - Year	Springer-Verlag 2009 (This will be the copyright line in the final PDF)	
Journal Name	Computational Mechanics	
Corresponding Author	Family Name	Chen
	Particle	
	Given Name	Jeng-Tzong
	Suffix	
	Division	Department of Harbor and River Engineering
	Organization	National Taiwan Ocean University
	Address	20224, Keelung, Taiwan
	Division	Department of Mechanical and Mechatronics Engineering
	Organization	National Taiwan Ocean University
	Address	20224, Keelung, Taiwan
	Email	jtchen@mail.ntou.edu.tw
Author	Family Name	Lee
	Particle	
	Given Name	Ying-Te
	Suffix	
	Division	Department of Harbor and River Engineering
	Organization	National Taiwan Ocean University
	Address	20224, Keelung, Taiwan
	Email	
Schedule	Received	27 October 2008
	Revised	
	Accepted	10 January 2009
Abstract	In this article, a systematic approach is proposed to calculate the torsional rigidity and stress of a circular bar containing multiple circular inclusions. To fully capture the circular geometries, the kernel function is expanded to the degenerate form and the boundary density is expressed into Fourier series. The approach is seen as a semi-analytical manner since error purely attributes to the truncation of Fourier series. By collocating the null-field point exactly on the real boundary and matching the boundary condition, a linear algebraic system is obtained. Convergence study shows that only a few number of Fourier series terms can yield acceptable results. Finally, torsion problems are revisited to check the validity of our method. Not only the torsional rigidities but also the stresses of multiple inclusions are also obtained by using the present approach.	
Keywords (separated by '-')	Torsional rigidity - Null-field integral equation - Degenerate kernel - Fourier series - Inclusion	
Footnote Information		

Journal: 466
Article: 305



Author Query Form

Please ensure you fill out your response to the queries raised below and return this form along with your corrections

Dear Author

During the process of typesetting your article, the following queries have arisen. Please check your typeset proof carefully against the queries listed below and mark the necessary changes either directly on the proof/online grid or in the 'Author's response' area provided below

Query	Details required	Author's response
1.	Kindly check and confirm whether the corresponding affiliation is okay.	

Torsional rigidity of a circular bar with multiple circular inclusions using the null-field integral approach

Jeng-Tzong Chen · Ying-Te Lee

Received: 27 October 2008 / Accepted: 10 January 2009
© Springer-Verlag 2009

Abstract In this article, a systematic approach is proposed to calculate the torsional rigidity and stress of a circular bar containing multiple circular inclusions. To fully capture the circular geometries, the kernel function is expanded to the degenerate form and the boundary density is expressed into Fourier series. The approach is seen as a semi-analytical manner since error purely attributes to the truncation of Fourier series. By collocating the null-field point exactly on the real boundary and matching the boundary condition, a linear algebraic system is obtained. Convergence study shows that only a few number of Fourier series terms can yield acceptable results. Finally, torsion problems are revisited to check the validity of our method. Not only the torsional rigidities but also the stresses of multiple inclusions are also obtained by using the present approach.

Keywords Torsional rigidity · Null-field integral equation · Degenerate kernel · Fourier series · Inclusion

1 Introduction

In the past, multiply-connected Laplace problems have been solved either by conformal mapping or by other techniques. Ling [14] solved the torsion problem of a circular bar with

several holes. Muskhelishvili [19] solved the problem of a circular bar reinforced by an eccentric circular inclusion. Chen and Weng [8] have introduced conformal mapping with a Laurent series expansion to analyze the Saint-Venant torsion problem. They concerned with an eccentric bar of different materials with an imperfect interface under torque. Since the conformal mapping is limited to the doubly-connected region, it encounters difficulty for multiple inclusions. Therefore, many researchers have paid more attentions on other techniques or numerical methods. In 1983, Caulk [3] developed a special boundary integral method to deal with the problem of a torsion bar with circular holes. Katsikadelis and Sapountzakis [11] used the boundary element method to solve the problem of an elliptic bar including one and two elliptic inclusions. Also, a practical problem of a rectangular concrete containing a Steel-I beam was concerned in their research. Later, Sapountzakis and Mokoš [22–24] extended to deal with the nonuniform torsion problem that the composite bar is subject to an arbitrarily concentrated or distributed twisting moment. Shams-Ahmadi and Chou [25] used the complex variable boundary element method (CVBEM) to solve the torsion problem of composite shafts with arbitrary number of inclusions of different materials. Ang and Kang [1] developed a general formulation for solving the second-order elliptic partial differential equation for a multiply-connected region in a different version of CVBEM. Petrov [21] developed an effective technique of boundary element method (BEM) to determine torsion, shear and other characteristics of beam cross-sections of arbitrary complex shape including multiply-connected cross sections. Tang [27] utilized the singular and hypersingular formulations to solve the torsion problem with inclusions and/or cracks.

Recently, meshless methods [10, 26] become very popular, since it is free of mesh generation and only nodes are needed. The present formulation can be seen as one kind of

J.-T. Chen (✉) · Y.-T. Lee
Department of Harbor and River Engineering,
National Taiwan Ocean University,
Keelung 20224, Taiwan
e-mail: jtchen@mail.ntou.edu.tw

J.-T. Chen
Department of Mechanical and Mechatronics Engineering,
National Taiwan Ocean University,
Keelung 20224, Taiwan

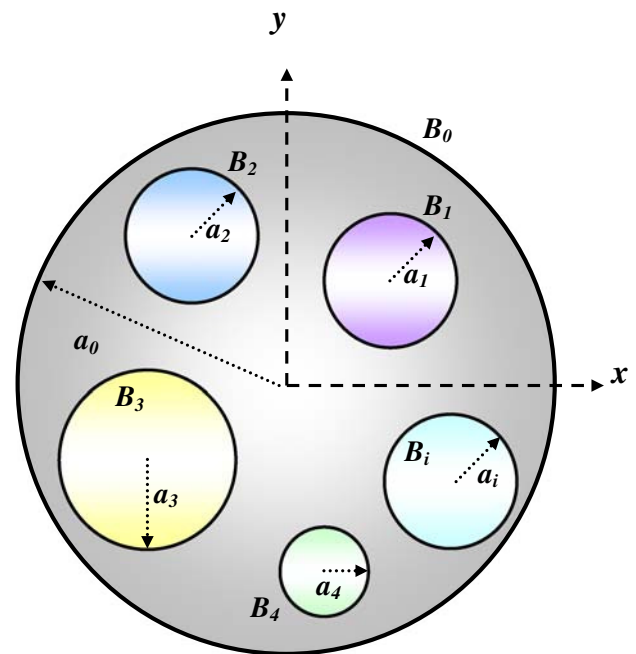


Fig. 1 Sketch of a circular bar with circular inclusions and/or holes under torsion

2 Formulation of the problem

A circular bar containing N circular inclusions bounded to the contours B_k ($k = 0, 1, 2, \dots, N$) is shown in Fig. 1. We define

$$B = \bigcup_{k=0}^N B_k. \tag{1}$$

The radii of circular bar and inclusions are a_0 and a_i ($i = 1, 2, \dots, N$), respectively. The circular bar twisted by couples applied at the end is taken into consideration. Following the theory of Saint-Venant torsion [28], we assume the displacement to be

$$u = -\alpha yz, \quad v = \alpha xz, \quad w = \alpha \varphi(x, y), \tag{2}$$

where α is the angle of twist per unit length along the z direction and φ is the warping function. The relation of strain and displacement is defined in the elasticity book [28] as shown below:

$$\begin{aligned} \varepsilon_x &= \frac{\partial u}{\partial x}, & \gamma_{xy} &= \frac{\partial u}{\partial y} + \frac{\partial v}{\partial x}, \\ \varepsilon_y &= \frac{\partial v}{\partial y}, & \gamma_{yz} &= \frac{\partial v}{\partial z} + \frac{\partial w}{\partial y}, \\ \varepsilon_z &= \frac{\partial w}{\partial z}, & \gamma_{zx} &= \frac{\partial w}{\partial x} + \frac{\partial u}{\partial z}. \end{aligned} \tag{3}$$

56 meshless methods, since only the collocation points on the
 57 real boundary are required to satisfy the boundary condition.
 58 Mogilevskaya and Crouch [16] have solved the problem of an
 59 infinite plane containing arbitrary number of circular inclu-
 60 sions based on the complex-variable singular integral
 61 equation. Later, they [9] utilized Somigliana's formula and
 62 Fourier series for elasticity problems with circular bound-
 63 aries. In their analysis procedure, the authors used the
 64 Fourier series to simulate the boundary densities on the cir-
 65 cular geometry. Besides, they used the complex variable and
 66 the residue theorem to calculate the singular integrals. There-
 67 fore, for calculating an integral over a circular boundary, they
 68 didn't expand the fundamental solution to degenerate kernel
 69 using the polar coordinate of local system. By moving the
 70 null-field point exactly on the real boundary, the boundary
 71 integral can be easily determined using series sums in our
 72 formulation due to the introduction of degenerate kernels.
 73 Also, it is free of worrying how to choose the collocation
 74 points, since uniform collocation along the circular bound-
 75 ary yields a well-conditioned matrix. Caulk [3] proposed a
 76 special BIEM to determine the torsional rigidity of a cir-
 77 cular bar with circular holes. He pointed out that Ling's result
 78 of three holes deviated from his data. Chen et al. [7] sup-
 79 ported the Caulk's comment by using the null-field integral
 80 approach. On the other hand, Bird and Steele [2] found the
 81 discrepancy between the Naghdi's solution [20] and their data
 82 for the beam bending problem with four holes. Also, Chen
 83 et al.'s result [4] agreed with the Naghdi's result. Following
 84 the success of [7], we extend to solve torsion problems with
 85 multiple circular inclusions. It is noted that we can deal with
 86 other shape of cross section in our approach, if the degenerate
 87 kernels corresponding to the special geometry are available.
 88 For example, degenerate kernel for the ellipse can be found
 89 in the book of Morse and Feshbach [17]. It is straightfor-
 90 ward to extend the present method to solve the problem with
 91 the geometry of an ellipse. Unfortunately, some formulae are
 92 not found in the mathematical handbook or were not derived
 93 by mathematicians for special geometry. That is to say, it is
 94 a challenging work in deriving the degenerate kernel for a
 95 special geometry case.
 96 In this paper, the null-field integral equation is utilized
 97 to solve the Saint-Venant torsion problem of a circular bar
 98 with circular inclusions. The mathematical tools, the degen-
 99 erate kernel for the fundamental solution and Fourier series
 100 for the boundary density, are utilized in the null-field inte-
 101 gral formulation. By collocating the null-field point exactly
 102 on the real boundary and matching the boundary condition,
 103 the linear algebraic system is obtained and the unknown
 104 Fourier coefficients can be easily determined. Then, series
 105 solutions for the warping function, torsional rigidity and
 106 stress are obtained. Convergence study is also addressed.
 107 Numerical examples are given to show the validity and effi-
 108 ciency of our formulation.

125 Then, substituting the displacement of Eq. 2 into Eq. 3, we
 126 have the strain components as follows:

$$\begin{aligned} \varepsilon_x = \varepsilon_y = \varepsilon_z = \gamma_{xy} = 0, \\ \gamma_{xz} = \alpha \left(\frac{\partial \varphi}{\partial x} - y \right), \\ \gamma_{yz} = \alpha \left(\frac{\partial \varphi}{\partial y} + x \right). \end{aligned} \tag{4}$$

128 By applying the Hooke's law, the stress components are

$$\begin{aligned} \sigma_x = \sigma_y = \sigma_z = \sigma_{xy} = 0, \\ \sigma_{xz} = \mu\alpha \left(\frac{\partial \varphi}{\partial x} - y \right), \\ \sigma_{yz} = \mu\alpha \left(\frac{\partial \varphi}{\partial y} + x \right), \end{aligned} \tag{5}$$

130 where μ is the shear modulus. There is no distortion in the
 131 planes of cross sections since $\varepsilon_x = \varepsilon_y = \varepsilon_z = \gamma_{xy} = 0$.
 132 We have the state of pure shear at each point defined by the
 133 stress components σ_{xz} and σ_{yz} . By substituting Eq. 5 to the
 134 equilibrium equation

$$\begin{aligned} \frac{\partial \sigma_x}{\partial x} + \frac{\partial \sigma_{xy}}{\partial y} + \frac{\partial \sigma_{xz}}{\partial z} + F_x = 0, \\ \frac{\partial \sigma_y}{\partial y} + \frac{\partial \sigma_{xy}}{\partial x} + \frac{\partial \sigma_{yz}}{\partial z} + F_y = 0, \\ \frac{\partial \sigma_z}{\partial z} + \frac{\partial \sigma_{xz}}{\partial x} + \frac{\partial \sigma_{yz}}{\partial y} + F_z = 0, \end{aligned} \tag{6}$$

136 the warping function satisfies the Laplace equation

$$\frac{\partial^2 \varphi}{\partial x^2} + \frac{\partial^2 \varphi}{\partial y^2} = 0 \quad \text{in } D, \tag{7}$$

138 where the body forces (F_x , F_y and F_z) are neglected and D
 139 is the domain of interest. On the cylinder surface, the stress
 140 states in Eq. 5 result in zero traction of $t_x = t_y = 0$. The only
 141 nonzero traction is t_z . Since there is no external traction, t_z ,
 142 on the cylindrical surface, we have

$$\begin{aligned} t_z = \sigma_{xz}n_x + \sigma_{yz}n_y \\ = \mu\alpha \left(\frac{\partial \varphi}{\partial x}n_x + \frac{\partial \varphi}{\partial y}n_y - yn_x + xn_y \right) = 0. \end{aligned} \tag{8}$$

145 Therefore, the bracket in Eq. 8 is equal to zero and we have
 146 the boundary condition as follows:

$$\frac{\partial \varphi}{\partial x}n_x + \frac{\partial \varphi}{\partial y}n_y = \nabla \varphi \cdot \mathbf{n} = \frac{\partial \varphi}{\partial n} = yn_x - xn_y. \tag{9}$$

148 For the ideal boundary between the matrix and inclusions,
 149 the continuity condition for the displacement and equilib-
 150 rium condition for traction on the interface [19] yield:

$$\varphi^M = \varphi^I \quad \text{on } B_i, \tag{10}$$

$$\mu_0 \frac{\partial \varphi_i^M}{\partial n} - \mu_i \frac{\partial \varphi_i^I}{\partial y} = (\mu_0 - \mu_i)(yn_x - xn_y) \quad \text{on } B_i, \tag{11}$$

154 where the superscripts "I" and "M" denote the inclusion and
 155 matrix, respectively, B_i is the i th interface boundary, μ_0 is
 156 the shear modulus for the matrix and μ_i is the shear modulus
 157 for the i th inclusion.

3 Method of solution

3.1 Dual null-field integral equations—the conventional version

161 The integral equation for the domain point can be derived
 162 from the third Green's identity [6], we have

$$\begin{aligned} 2\pi \varphi(x) = \int_B T(s, x) \varphi(s) dB(s) \\ - \int_B U(s, x) \psi(s) dB(s), \quad x \in D, \end{aligned} \tag{12}$$

$$\begin{aligned} 2\pi \frac{\partial \varphi(x)}{\partial n_x} = \int_B M(s, x) \varphi(s) dB(s) \\ - \int_B L(s, x) \psi(s) dB(s), \quad x \in D, \end{aligned} \tag{13}$$

167 where s and x are the source and field points, respectively,
 168 D is the domain of interest, $\psi(s) = \frac{\partial \varphi(s)}{\partial n_s}$, n_s and n_x denote
 169 the outward normal vectors at the source point s and field
 170 point x , respectively, and the kernel function $U(s, x) = \ln r$,
 171 ($r \equiv |s - x|$), is the fundamental solution which satisfies

$$\nabla^2 U(s, x) = 2\pi \delta(x - s) \tag{14}$$

173 in which $\delta(x - s)$ denotes the Dirac-delta function. The other
 174 kernel functions, $T(s, x)$, $L(s, x)$, and $M(s, x)$, are defined
 175 by

$$T(s, x) = \frac{\partial U(s, x)}{\partial n_s}, \tag{15}$$

$$L(s, x) = \frac{\partial U(s, x)}{\partial n_x}, \tag{16}$$

$$M(s, x) = \frac{\partial^2 U(s, x)}{\partial n_s \partial n_x}. \tag{17}$$

Author Proof

179 By moving the field point to the boundary, Eqs. 12 and 13
 180 reduce to

$$181 \quad \pi \varphi(x) = C.P.V. \int_B T(s, x) \varphi(s) dB(s) \\
 182 \quad - R.P.V. \int_B U(s, x) \psi(s) dB(s), \quad x \in B, \quad (18)$$

$$183 \quad \pi \frac{\partial \varphi(x)}{\partial n_x} = H.P.V. \int_B M(s, x) \varphi(s) dB(s) \\
 184 \quad - C.P.V. \int_B L(s, x) \psi(s) dB(s), \quad x \in B, \quad (19)$$

185 where *R.P.V.*, *C.P.V.* and *H.P.V.* denote the Riemann
 186 principal value, Cauchy principal value and Hadamard prin-
 187 cipal value, respectively. Once the field point *x* locates
 188 outside the domain ($x \in D^c$), we obtain the dual null-field
 189 integral equations as shown below

$$190 \quad 0 = \int_B T(s, x) \varphi(s) dB(s) \\
 191 \quad - \int_B U(s, x) \psi(s) dB(s), \quad x \in D^c, \quad (20)$$

$$192 \quad 0 = \int_B M(s, x) \varphi(s) dB(s) \\
 193 \quad - \int_B L(s, x) \psi(s) dB(s), \quad x \in D^c, \quad (21)$$

194 where D^c is the complementary domain. Equations 12, 13,
 195 20 and 21 are conventional formulations where the point can
 196 not be located on the real boundary. Singularity occurs and
 197 concept of principal values is required once Eqs. 18 and 19
 198 are considered.

199 3.2 Dual null-field integral formulation—the present 200 version

201 By introducing the degenerate kernels, the collocation point
 202 can be located on the real boundary free of facing singu-
 203 larity. Therefore, the representations of integral equations
 204 including the boundary point for the interior problem can be
 205 written as

$$206 \quad 2\pi \varphi(x) = \int_B T^i(s, x) \varphi(s) dB(s) \\
 207 \quad - \int_B U^i(s, x) \psi(s) dB(s), \quad x \in D \cup B, \quad (22)$$

$$208 \quad 2\pi \frac{\partial \varphi(x)}{\partial n_x} = \int_B M^i(s, x) \varphi(s) dB(s) \\
 209 \quad - \int_B L^i(s, x) \psi(s) dB(s), \quad x \in D \cup B, \quad (23)$$

210 and

$$211 \quad 0 = \int_B T^e(s, x) \varphi(s) dB(s) \\
 212 \quad - \int_B U^e(s, x) \psi(s) dB(s), \quad x \in D^c \cup B, \quad (24)$$

$$213 \quad 0 = \int_B M^e(s, x) \varphi(s) dB(s) \\
 214 \quad - \int_B L^e(s, x) \psi(s) dB(s), \quad x \in D^c \cup B, \quad (25)$$

215 once the kernels are expressed in term of an appropriate
 216 degenerate forms (denoted by subscripts *i* and *e*) instead of
 217 the closed-form fundamental solution without distinction. It
 218 is noted that *x* in Eqs. 22–25 can exactly be located on the
 219 real boundary. For the exterior problem, the domain of inter-
 220 est is in the external region of the circular boundary and the
 221 complementary domain is in the internal region of the circle.
 222 Therefore, the null-field integral equations are represented as

$$223 \quad 2\pi \varphi(x) = \int_B T^e(s, x) \varphi(s) dB(s) \\
 224 \quad - \int_B U^e(s, x) \psi(s) dB(s), \quad x \in D \cup B, \quad (26)$$

$$225 \quad 2\pi \frac{\partial \varphi(x)}{\partial n_x} = \int_B M^e(s, x) \varphi(s) dB(s) \\
 226 \quad - \int_B L^e(s, x) \psi(s) dB(s), \quad x \in D \cup B, \quad (27)$$

227 and

$$228 \quad 0 = \int_B T^i(s, x) \varphi(s) dB(s) \\
 229 \quad - \int_B U^i(s, x) \psi(s) dB(s), \quad x \in D^c \cup B, \quad (28)$$

$$230 \quad 0 = \int_B M^i(s, x) \varphi(s) dB(s) \\
 231 \quad - \int_B L^i(s, x) \psi(s) dB(s), \quad x \in D^c \cup B, \quad (29)$$

232 Also, *x* in Eqs. 26–29 can exactly be located on the real
 233 boundary. For various problems (interior or exterior), we
 234 used different kernel functions (denoted by superscripts “*i*”

235 and “e”) so that jump behavior across the boundary can be
 236 captured. Therefore, different expressions of the kernels for
 237 the interior and exterior observer points are used and they
 238 will be elaborated on latter.

239 It is worthy of noting that our approach can yield the
 240 same linear algebraic equation derived from boundary integral
 241 equation in Eqs. 18 and 19. However, the procedure is
 242 quite different although collocation points are located on the
 243 real boundary for both the conventional BIEM and the present
 244 approach. For the conventional BEM, it is necessary to
 245 calculate the singular or hypersingular integral by using the
 246 sense of principal value. Our approach is free of calculating
 247 principal value due to the introduction of the degenerate
 248 kernel since the kernel functions were separated into two
 249 parts, interior and exterior parts. If the appropriate kernels
 250 (interior and exterior parts) are chosen, we can easily obtain
 251 the same linear algebraic equation derived from the conventional
 252 BIE and free of calculating principal value.

253 3.3 Expansions of fundamental solution and boundary
 254 density

255 Based on the separable property, the kernel function $U(s, x)$
 256 can be expanded into degenerate form by separating the
 257 source points and field points in the polar coordinate [5]:

258 $U(s, x)$

$$= \begin{cases} U^i(R, \theta; \rho, \phi) = \ln R - \sum_{m=1}^{\infty} \frac{1}{m} \left(\frac{\rho}{R}\right)^m \cos m(\theta - \phi), \\ R \geq \rho, \\ U^e(R, \theta; \rho, \phi) = \ln \rho - \sum_{m=1}^{\infty} \frac{1}{m} \left(\frac{R}{\rho}\right)^m \cos m(\theta - \phi), \\ R < \rho, \end{cases}, \quad (30)$$

261 where the superscripts “i” and “e” denote the interior
 262 ($R \geq \rho$) and exterior ($R < \rho$) cases, respectively. In order
 263 to ensure the log singularity and the series convergence, the
 264 leading term and the numerator in the above expansion is
 265 dominated by the larger argument. After taking the deriva-
 266 tive operators in Eqs. 15-17, $T(s, x)$, $L(s, x)$ and $M(s, x)$
 267 kernels can be easily derived and the detailed representation
 268 can be found in [7]. It is noted that the null-field point or
 269 the domain point can be exactly located on the real boundary
 270 when the appropriate degenerate kernels are employed. The
 271 main advantage of present formulation is that the collocation
 272 point x is located on the real boundary free of singular
 273 integrals, while the conventional BEM needs to deal with sin-
 274 gularities since a closed-form kernel is used. Therefore, the
 275 main difference between our approach and the conventional
 276 method is that we don’t use the bump contour approach on the
 277 integration path to obtain free term. Furthermore, the jump

278 behavior for potentials of integral equations between the
 279 domain point and the null-field point is captured when various
 280 degenerate kernels for fundamental solutions are employed
 281 for the domain point and complementary domain point. In
 282 other words, the jump behavior is revealed by using various
 283 degenerate kernels for the fundamental solution instead of
 284 employing the bump contour approach in the conventional
 285 boundary integral equation method.

286 For the boundary densities, we apply the Fourier series
 287 expansions to approximate the potential φ and its normal
 288 derivative ψ on the boundary

$$\varphi(s_k) = a_0^k + \sum_{n=1}^{\infty} (a_n^k \cos n\theta + b_n^k \sin n\theta), \quad (31)$$

$$s_k \in B_k, \quad k = 1, 2, \dots, N,$$

$$\psi(s_k) = p_0^k + \sum_{n=1}^{\infty} (p_n^k \cos n\theta + q_n^k \sin n\theta), \quad (32)$$

$$s_k \in B_k, \quad k = 1, 2, \dots, N,$$

293 where a_n^k, b_n^k, p_n^k and q_n^k are the Fourier coefficients and θ is
 294 the polar angle ($0 < \theta < 2\pi$).

295 3.4 Linear algebraic system

296 After locating the null-field point x_k exactly on the k th cir-
 297 cular boundary in Eq. 24 or Eq. 28 as shown in Fig. 2, we
 298 have

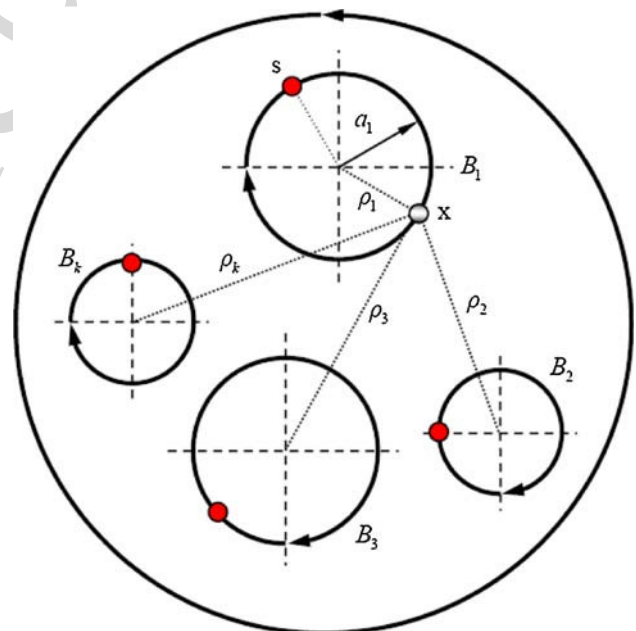


Fig. 2 Sketch of the null-field integral equation in conjunction with the adaptive observer system

$$0 = \sum_{k=0}^N \int_{B_k} T(s, x) \varphi(s) dB_k(s) - \sum_{k=0}^N \int_{B_k} U(s, x) \psi(s) dB_k(s), \quad x \in D^c \cup B, \quad (33)$$

where N is the number of circles including the outer boundary and the inner circular holes. Since the boundary integral equations are frame indifferent, i.e. objectivity rule is satisfied. The origin of observer system is adaptively chosen at the center of circular boundary under integration. The dummy variable in the circular integration is angle (θ) instead of radial coordinate (R). In the real computation, we select the collocation point on the boundary and the integration path is counterclockwise for the outer circle. Otherwise, it is clockwise. For the B integral of the circular boundary, the kernels of $U(s, x)$ and $T(s, x)$ are expressed in terms of degenerate kernels, and $\varphi(s)$ and $\psi(s)$ are substituted by using the Fourier series. In the B_k integral, we set the origin of the

$$\{\varphi\} = \begin{Bmatrix} \varphi_0 \\ \varphi_1 \\ \varphi_2 \\ \vdots \\ \varphi_N \end{Bmatrix}, \quad \{\psi\} = \begin{Bmatrix} \psi_0 \\ \psi_1 \\ \psi_2 \\ \vdots \\ \psi_N \end{Bmatrix} \quad (37)$$

where the vectors $\{\varphi_k\}$ and $\{\psi_k\}$ are in the forms of $\{a_0^k a_1^k b_1^k \dots a_L^k b_L^k\}^T$ and $\{p_0^k p_1^k q_1^k \dots p_L^k q_L^k\}^T$, respectively; the first subscript “ j ” ($j = 0, 1, 2, \dots, N,$) in $[U_{jk}]$ and $[T_{jk}]$ denotes the index of the j th circle where the collocation point is located and the second subscript “ k ” ($k = 0, 1, 2, \dots, N,$) denotes the index of the k th circle where the boundary data $\{\varphi_k\}$ and $\{\psi_k\}$ are specified and L indicates the truncated terms of Fourier series. The coefficient matrix of the linear algebraic system is partitioned into blocks, and each off-diagonal block corresponds to the influence matrices between two different circular holes. The diagonal blocks are the influence matrices due to itself in each individual hole. After uniformly collocating the null-field point along the k th circular boundary, the submatrix can be written as

$$[\mathbf{K}_{jk}] = \begin{bmatrix} K_{jk}^{0c}(\phi_1) & K_{jk}^{1c}(\phi_1) & K_{jk}^{1s}(\phi_1) & \dots & K_{jk}^{Mc}(\phi_1) & K_{jk}^{Ms}(\phi_1) \\ K_{jk}^{0c}(\phi_2) & K_{jk}^{1c}(\phi_2) & K_{jk}^{1s}(\phi_2) & \dots & K_{jk}^{Mc}(\phi_2) & K_{jk}^{Ms}(\phi_2) \\ K_{jk}^{0c}(\phi_3) & K_{jk}^{1c}(\phi_3) & K_{jk}^{1s}(\phi_3) & \dots & K_{jk}^{Mc}(\phi_3) & K_{jk}^{Ms}(\phi_3) \\ \vdots & \vdots & \vdots & \ddots & \vdots & \vdots \\ K_{jk}^{0c}(\phi_{2L}) & K_{jk}^{1c}(\phi_{2L}) & K_{jk}^{1s}(\phi_{2L}) & \dots & K_{jk}^{Mc}(\phi_{2L}) & K_{jk}^{Ms}(\phi_{2L}) \\ K_{jk}^{0c}(\phi_{2L+1}) & K_{jk}^{1c}(\phi_{2L+1}) & K_{jk}^{1s}(\phi_{2L+1}) & \dots & K_{jk}^{Mc}(\phi_{2L+1}) & K_{jk}^{Ms}(\phi_{2L+1}) \end{bmatrix}, \quad (38)$$

observer system to collocate at the center c_k to fully utilize the degenerate kernels and Fourier series. By collocating the null-field point exactly on the boundary, a linear algebraic system is obtained

$$[\mathbf{U}]\{\psi\} = [\mathbf{T}]\{\varphi\}, \quad (34)$$

where $[\mathbf{U}]$ and $[\mathbf{T}]$ are the influence matrices with a dimension of $N \times (2L + 1)$ by $N \times (2L + 1)$, $\{\varphi\}$ and $\{\psi\}$ denote the column vectors of Fourier coefficients with a dimension of $N \times (2L + 1)$ by 1 in which $[\mathbf{U}]$, $[\mathbf{T}]$, $\{\varphi\}$ and $\{\psi\}$ can be defined as follows:

$$[\mathbf{U}] = \begin{bmatrix} \mathbf{U}_{00} & \mathbf{U}_{01} & \dots & \mathbf{U}_{0N} \\ \mathbf{U}_{10} & \mathbf{U}_{11} & \dots & \mathbf{U}_{1N} \\ \vdots & \vdots & \ddots & \vdots \\ \mathbf{U}_{N0} & \mathbf{U}_{N0} & \dots & \mathbf{U}_{NN} \end{bmatrix}, \quad (35)$$

$$[\mathbf{T}] = \begin{bmatrix} \mathbf{T}_{00} & \mathbf{T}_{01} & \dots & \mathbf{T}_{0N} \\ \mathbf{T}_{10} & \mathbf{T}_{11} & \dots & \mathbf{T}_{1N} \\ \vdots & \vdots & \ddots & \vdots \\ \mathbf{T}_{N0} & \mathbf{T}_{N1} & \dots & \mathbf{T}_{NN} \end{bmatrix}, \quad (36)$$

where K can be substituted by U or T . Although the matrix in Eq. 38 is not sparse, it is diagonally dominant. It is found that the influence coefficient for the higher-order harmonics is smaller. It is noted that the superscript “0s” in Eq. 38 disappears since $\sin(0\theta) = 0$. The element of $[\mathbf{K}_{jk}]$ is defined, respectively, as

$$K_{jk}^{nc}(\phi_m) = \int_{B_k} K(s_k, x_m) \cos(n\theta_k) R_k d\theta_k, \quad (39)$$

$$K_{jk}^{ns}(\phi_m) = \int_{B_k} K(s_k, x_m) \sin(n\theta_k) R_k d\theta_k, \quad (40)$$

where $n = 0, 1, 2, \dots, L, m = 1, 2, \dots, 2L + 1$, and ϕ_m is the polar angle of the collocating points x_m along the boundary. The physical meaning of the influence coefficient for $U_{jk}^{nc}(\phi_m)$ in Eq. 39 denotes the response at x_m due to the $\cos(n\theta)$ distribution. By rearranging the known and unknown sets, the unknown Fourier coefficients are determined. Equation 24 can be calculated by employing the orthogonal relations of trigonometric functions in the real computation.

358 Only the finite L terms are used in the summation of Eqs. 31
 359 and 32.

360 By using the concept of domain decomposition, the problem
 361 in Fig. 1 can be decomposed into two parts as shown in
 362 Figs. 3(a) and 3(b). One is the torsion problem of a circular
 363 bar with multiple circular holes and the other is a problem of
 364 each inclusion. For the torsion problem with circular holes
 365 which satisfies the Laplace equation, the linear algebraic system
 366 from Eq. 34 can be obtained as

$$\begin{bmatrix} \mathbf{T}_{00}^M & \mathbf{T}_{01}^M & \dots & \mathbf{T}_{0N}^M & -\mathbf{U}_{01}^M & \dots & -\mathbf{U}_{0N}^M \\ \mathbf{T}_{10}^M & \mathbf{T}_{11}^M & \dots & \mathbf{T}_{1N}^M & -\mathbf{U}_{11}^M & \dots & -\mathbf{U}_{1N}^M \\ \vdots & \vdots & \ddots & \vdots & \vdots & \ddots & \vdots \\ \mathbf{T}_{N0}^M & \mathbf{T}_{N1}^M & \dots & \mathbf{T}_{NN}^M & -\mathbf{U}_{N1}^M & \dots & -\mathbf{U}_{NN}^M \end{bmatrix} \begin{bmatrix} \varphi_0^M \\ \varphi_1^M \\ \vdots \\ \varphi_N^M \\ \psi_1^M \\ \vdots \\ \psi_N^M \end{bmatrix} = \begin{bmatrix} \mathbf{0} \\ \mathbf{0} \\ \vdots \\ \mathbf{0} \end{bmatrix}. \tag{41}$$

369 For each inclusion, we have

$$\begin{bmatrix} \mathbf{T}_{11}^I & \mathbf{0} & \mathbf{0} & -\mathbf{U}_{11}^I & \mathbf{0} & \mathbf{0} \\ \mathbf{0} & \ddots & \mathbf{0} & \mathbf{0} & \ddots & \mathbf{0} \\ \mathbf{0} & \mathbf{0} & \mathbf{T}_{NN}^I & \mathbf{0} & \mathbf{0} & -\mathbf{U}_{NN}^I \end{bmatrix} \begin{bmatrix} \varphi_1^I \\ \vdots \\ \varphi_N^I \\ \psi_1^I \\ \vdots \\ \psi_N^I \end{bmatrix} = \begin{bmatrix} \mathbf{0} \\ \vdots \\ \mathbf{0} \end{bmatrix}. \tag{42}$$

372 In order to satisfy the continuity conditions of displacement
 373 and equilibrium condition of traction on the interface, we
 374 have

$$\{\varphi_i^M\} - \{\varphi_i^I\} = \{\mathbf{0}\}, \tag{43}$$

$$\mu_0 \{\psi_i^M\} - \mu_i \{\psi_i^I\} = \{\mathbf{b}^i\}, \tag{44}$$

377 where $\{\mathbf{b}^i\}$ is

$$\{\mathbf{b}^i\} = \left\{ \begin{array}{l} (\mu_0 - \mu_i)(e_y^i \cos \theta_1^i - e_x^i \sin \theta_1^i) \\ (\mu_0 - \mu_i)(e_y^i \cos \theta_2^i - e_x^i \sin \theta_2^i) \\ \vdots \\ (\mu_0 - \mu_i)(e_y^i \cos \theta_{2M}^i - e_x^i \sin \theta_{2M}^i) \\ (\mu_0 - \mu_i)(e_y^i \cos \theta_{2M+1}^i - e_x^i \sin \theta_{2M+1}^i) \end{array} \right\}. \tag{45}$$

379

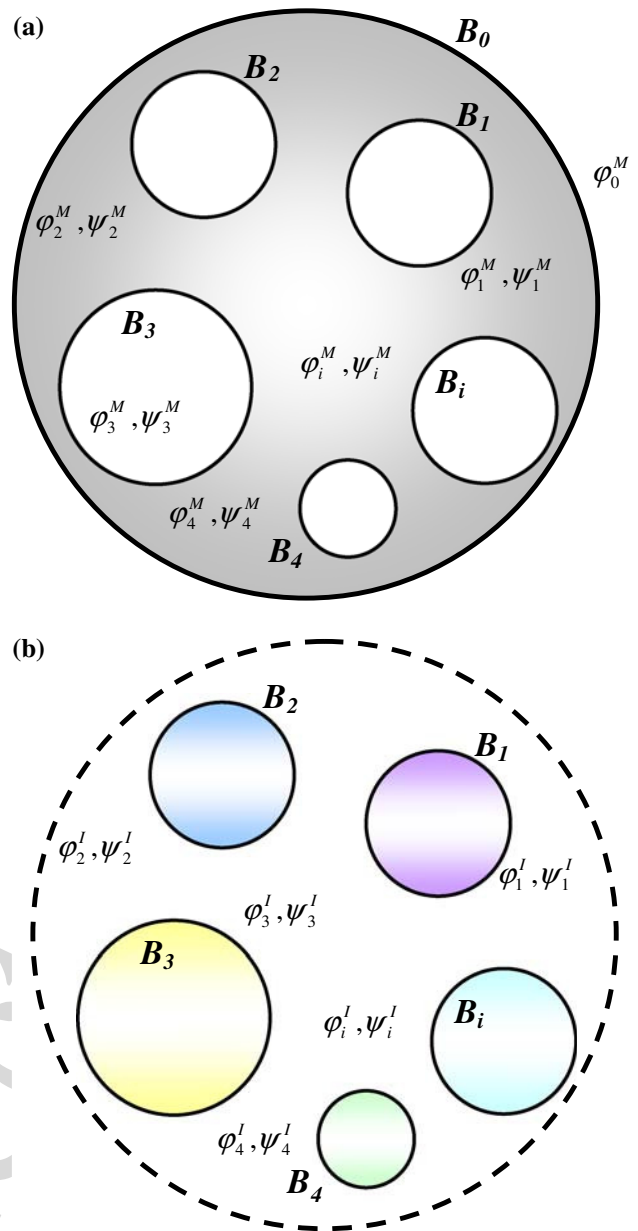


Fig. 3 a Torsion problem of a circular bar with circular holes. b Each circular inclusion problem

380 Combining with the above mentioned linear algebraic system of Eqs. 41–44, the global linear algebraic equation is obtained by correctly arranging the Fourier coefficients. After obtaining the Fourier coefficients, the torsional rigidity can be easily determined as follows: 381 382 383 384

$$G = \mu \int_D (x^2 + y^2) dD - \mu \sum_{k=1}^N \int_{B_k} \varphi \frac{\partial \varphi}{\partial n} dB_k, \tag{46}$$

$$G^T = G^M + G^I, \tag{47}$$

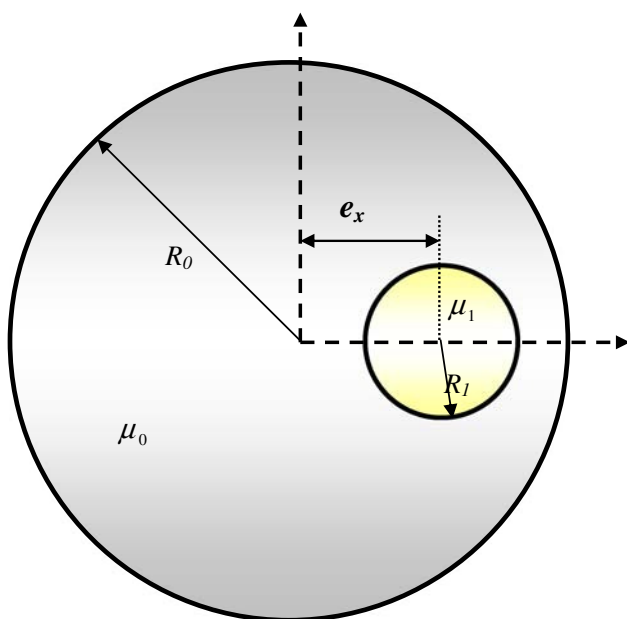


Fig. 4 Sketch of an eccentric circular inclusion problem

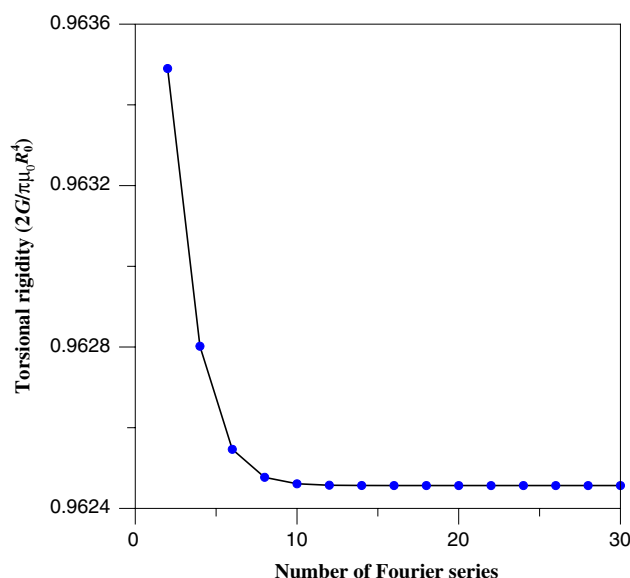


Fig. 5 Torsional rigidity versus the number of Fourier series terms

where the subscripts of "T", "M" and "I" denote the torsion rigidity of total, matrix and inclusion, respectively.

4 Illustrative examples and discussions

In this section, we revisit the torsion problems with inclusions and/or holes which have been solved by Muskhelishvili [19], Petrov [21], Tang [27], Ling [14], and Kuo and Conway [12, 13] for demonstrating the validity of present method. The torsional rigidity of each example is calculated after determining the unknown Fourier coefficients.

Example 1 A circular bar with an eccentric inclusion.

A circular bar of radius R_0 with an eccentric circular inclusion of radius R_1 is shown in Fig. 4. The ratio of R_1/R_0 and e_x/R_0 are 0.3 and 0.6, respectively. Fig. 5 shows the torsional rigidity versus the number of Fourier series term when μ_1/μ_0 is equal to 0.6. It is found that the solution converges fast by using only fourteen terms of Fourier series. The results of torsional rigidity for different values of μ_1/μ_0 are shown in Table 1. For verifying our results, the Muskhelishvili's solution [19] is shown below,

$$G = \mu_0 I + (\mu_1 - \mu_0) I' - \frac{\pi R_1^2 e_x^2 (\mu_1 - \mu_0)^2}{\mu_1 + \mu_0} - 2\mu_0 \pi e_x^2 \nu \rho_1^2 \sum_{k=1}^{\infty} \frac{\alpha^k \nu^k}{(1 - a^2 \rho_1^2 \alpha^k)^2}, \quad (48)$$

where $I = (\pi R_0^4/2)$, $I' = (\pi R_1^4/2) + \pi R_1^2 e_x^2$, $a = e_x / (\sqrt{(R_1^2 - R_0^2)^2 - 2e_x^2(R_1^2 + R_0^2) + e_x^4})$, $\alpha = (\rho_1^2/\rho_0^2)$, $\nu = ((\mu_0 - \mu_1)/(\mu_0 + \mu_1))$, $\rho_1 = (\sqrt{1 + 4R_1^2 a^2} - 1/2R_1 a^2)$ and $\rho_0 = (\sqrt{1 + 4R_0^2 a^2} - 1/2R_0 a^2)$. The exact solution of Muskhelishvili and the result of integral formulation by Tang [27] are shown in Table 1 for comparison. The present results match very well with the exact solution derived by Muskhelishvili and are better than those of Tang [27]. For the rigid inclusion, the torsional rigidity becomes infinity as shown in Table 1. Fig. 6 is shown to indicate how shear modulus of inclusion influences the torsional rigidity. It is observed that the slope of torsional rigidity versus μ_1 is $(R_1/R_0)^4$ when the shear modulus of the inclusion becomes large. This finding is expected according to Eq. 44.

Example 2 A circular bar with one circular hole (limiting case).

The problem is different with the Case 1 by setting zero modulus of the inclusion to simulate the hole in our program. The limiting case is used to check the present formulation. The radius of a circular bar is 1.0 and the radius of the hole is 0.3. The eccentricity ($e_x = 0.5$) is considered. The shear moduli μ_0 and μ_1 are chosen 1.0 and 0, respectively. The exact solution of Muskhelishvili [19] is also calculated by using the exact formula. The results are shown in Table 2. It is found that the results of present method matches well with those of the Muskhelishvili's data [19] and are better than those of the Petrov's results [21]. However, the Lurje's solution [15] is smaller than those of the Petrov's, Muskhelishvili's and our results. Since three various

Table 1 Torsional rigidity of a circular bar with an eccentric inclusion

$\frac{\mu_1}{\mu_0}$	$2G/\pi\mu_0R_0^4$		
	Muskhelishvili [19]	Tang [27]	Present method ($M = 20$)
0	0.82370	0.82377	0.82370
0.2	0.89180	0.89181	0.89180
0.6	0.96246	0.96246	0.96246
1.0	1.00000	1.00000	1.00000
5.0	1.10800	1.10794	1.10800
20.0	1.25224	1.25181	1.25224
1000	9.19866	N/A	9.19866
10000	82.09883	N/A	82.09882
1000000	8101.10012	N/A	8101.09883

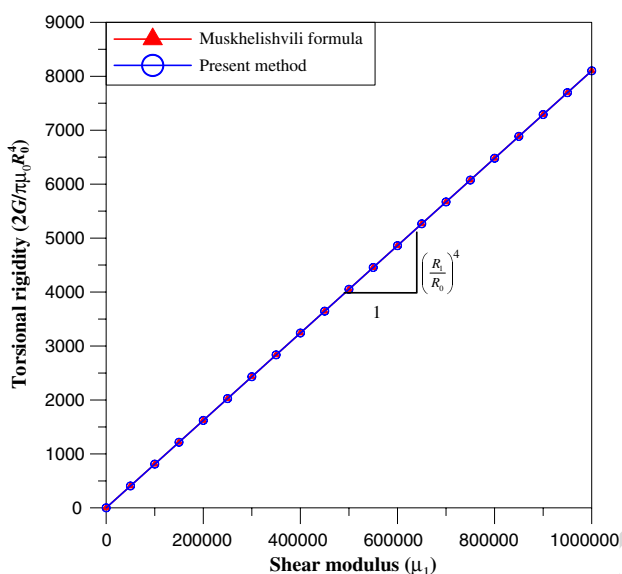


Fig. 6 Torsional rigidity versus the shear modulus of inclusion

Table 2 Torsional rigidity of a circular bar with an eccentric hole

	$G/\mu_0R_0^4$		
Present method	1.389 (34)	1.389 (66)	1.389 (130)
Petrov [21]	1.391 (32)	1.390 (64)	1.389 (130)
Lurje [15]	1.311		
Muskhelishvili [19]	1.389		

The data in the parenthesis denotes number of degrees of freedom

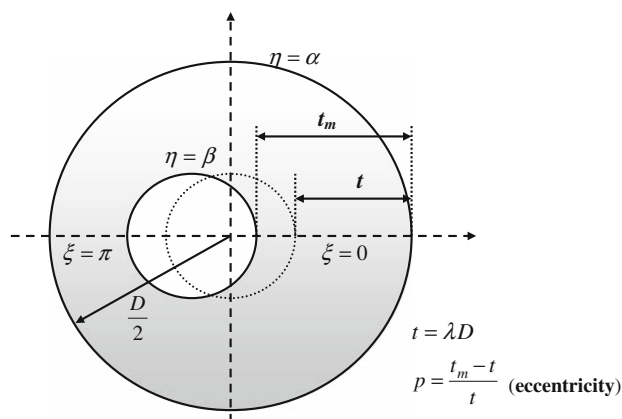


Fig. 7 Sketch of eccentric problem

$$\xi_z = \mu_0\alpha \frac{\partial\varphi}{\partial\eta}. \tag{49}$$

By using the chain rule, we can obtain the following relation

$$\xi_z = \mu_0\alpha \left(\frac{\partial\varphi}{\partial x} \frac{\partial x}{\partial\eta} + \frac{\partial\varphi}{\partial y} \frac{\partial y}{\partial\eta} \right), \tag{50}$$

where $x = \frac{a \sinh \eta}{\cosh \eta - \cos \xi}$, $y = \frac{a \sin \xi}{\cosh \eta - \cos \xi}$ and a in our case is 1.58016. The stresses along the inner and outer boundaries for $\lambda = 0.3$ and $p = 0.4$ are shown in Table 3. It is found that the errors are less than two percents. The stresses on the x axis in domain are shown in Table 4. The results are very close to the Ling’s analytical results obtained from the bipolar coordinate system.

Example 3 A circular rod with a ring of circular inclusions.

In this example, we revisit the problems of a circular rod with a ring of circular inclusions investigated by Kuo and Conway [12] as shown in Fig. 8. Three cases are given in their article as

Case 1: $\frac{b}{a} = \frac{3}{4}, \frac{\lambda}{a} = \frac{1}{8}, \frac{\delta}{a} = \frac{1}{2}, \frac{G_2}{G_1} = 30, k = 8,$

Case 2: $\frac{b}{a} = \frac{3}{4}, \frac{\lambda}{a} = \frac{1}{8}, \frac{\delta}{a} = \frac{1}{2}, \frac{G_2}{G_1} = 5, k = 3,$

Case 3: $\frac{b}{a} = \frac{1}{2}, \frac{\lambda}{a} = \frac{1}{4}, \frac{\delta}{a} = 0, \frac{G_2}{G_1} = 29.4, k = 4.$

The results of the present approach are shown in Table 5. It is found that the results of our approach are slightly different from the Kuo and Conway’s results. For the Case 3, Kuo and Conway [12] claimed that they obtained the nondimensional torsional rigidity 1.57 analytically and 1.53 in the experiment. It seems that they obtained consistent results. However, the data of FE solution 1.77 obtained by Murakami and Yamakawa [18] agrees well with the result of our approach. In this case, our result deviates from the experiment data of Kuo and Conway [12] but converges to the data of finer mesh using FEM by Murakami and Yamakawa [18]. Both our result and that of Murakami and Yamakawa

methods obtain the consistent result, the formulae of Lurje [15] needs further check.

The stress analysis has been done by Ling [14]. The corresponding parameters are shown in Fig. 7. The definition of shear stress component, ξ_z , is shown below

Table 3 ξ_z on the boundary for $\lambda = 0.3$ and $p = 0.4$

ξ	$\eta = \alpha$			$\eta = \beta$		
	θ	$\frac{2}{\mu\tau D}\xi_z[14]$	Present method	θ	$\frac{2}{\mu\tau D}\xi_z[14]$	Present method
π	180°	1.166	1.166	180°	1.015	1.012
$\frac{3}{4}\pi$	$154^\circ 18'$	1.115	1.114	$144^\circ 16'$	0.881	0.881
$\frac{1}{2}\pi$	$122^\circ 19'$	1.011	1.011	$104^\circ 12'$	0.522	0.522
$\frac{1}{4}\pi$	$73^\circ 55'$	0.949	0.949	$56^\circ 2'$	0.068	0.067
0	0°	0.936	0.940	0°	-0.166	-0.167

Table 4 ξ_z along the line of $\xi = 0$ and π for $\lambda = 0.3$ and $p = 0.4$

η	$\xi = \pi$			$\xi = 0$		
	$\frac{x_1}{D}$	$\frac{2}{\mu\tau D}\xi_z[14]$	Present method	$\frac{x_2}{D}$	$\frac{2}{\mu\tau D}\xi_z[14]$	Present method
1.2384	0	1.166	1.166	0	0.940	0.940
1.4084	0.0446	1.097	1.096	0.1335	0.652	0.651
1.5784	0.0848	1.044	1.043	0.2342	0.420	0.418
1.7484	0.1208	1.009	1.010	0.3120	0.215	0.216
1.9784	0.1528	0.998	0.999	0.3730	0.026	0.026
2.0826	0.1800	1.015	1.012	0.4200	-0.166	-0.167

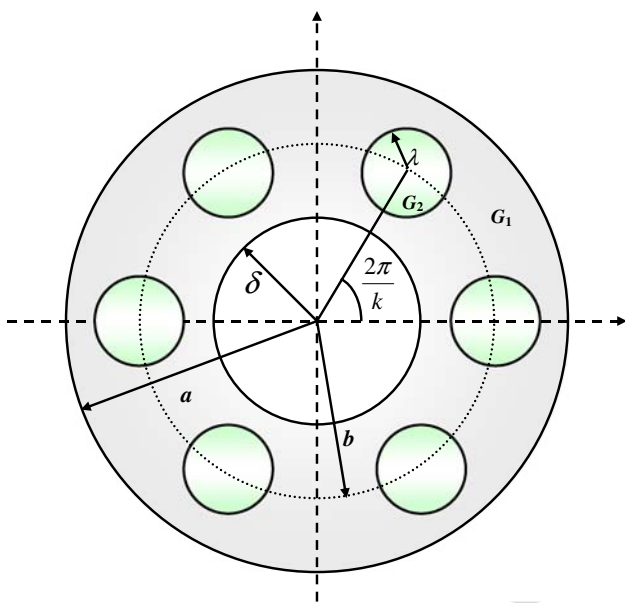


Fig. 8 A circular rod with a ring of circular inclusions

numerical result may not be correct if the two results deviate. As we know, the mathematical model is established under certain assumptions. Therefore, the mathematical model is always simpler than the real problem. If the mathematical model has the analytical or exact solution, it is the basic solution for comparison with the numerical result. For the real problem, many uncertain conditions exist in the experiment. Valid experimental data need special care. The inconsistency between the experimental data and numerical results stems from many reasons. So, the mathematical model is continuously modified by adding specific consideration.

Example 4 A circular rod with several rings of circular inclusions.

In this example, we consider a circular rod with several rings of circular inclusions proposed by Kuo and Conway [13]. Four cases were addressed

- Case 1: $\frac{b_1}{a} = \frac{3}{8}, \frac{b_2}{a} = \frac{3}{4}, \frac{\lambda}{a} = \frac{1}{8}, \frac{G}{G_0} = 30, j = 2, k = 6,$
- Case 2: $\frac{b_1}{a} = \frac{1}{4}, \frac{b_2}{a} = \frac{17}{32}, \frac{b_3}{a} = \frac{13}{16}, \frac{\lambda}{a} = \frac{3}{32}, \frac{G}{G_0} = 30, j = 3, k = 6,$
- Case 3: $\frac{b_1}{a} = \frac{3}{8}, \frac{b_2}{a} = \frac{3}{4}, \frac{\lambda}{a} = \frac{1}{8}, \frac{G}{G_0} = 0, j = 2, k = 6,$
- Case 4: $\frac{b_1}{a} = \frac{1}{4}, \frac{b_2}{a} = \frac{17}{32}, \frac{b_3}{a} = \frac{13}{16}, \frac{\lambda}{a} = \frac{3}{32}, \frac{G}{G_0} = 0, j = 3, k = 6.$

may open the issue that Kuo and Conway's result may be questionable. In general, the numerical analysis is developed to predict the data before experiment. However, we always find that the results have differences between the numerical analysis and experiment data. We may wonder that the

Author Proof

Table 5 Torsional rigidity of different cases for a circular ring with inclusions

Case	$\frac{b}{a}$	$\frac{\lambda}{a}$	$\frac{\delta}{a}$	$\frac{G_2}{G_1}$	k	$\frac{G_e}{G_1}$ [12]	$\frac{G_e}{G_1}$ (present)
Case 1	$\frac{3}{4}$	$\frac{1}{8}$	$\frac{1}{2}$	30	8	1.2330	1.2924
Case 2	$\frac{3}{4}$	$\frac{1}{8}$	$\frac{1}{2}$	5	3	1.0466	1.0742
Case 3	$\frac{1}{2}$	$\frac{1}{4}$	0	29.4	4	1.5706	1.7740

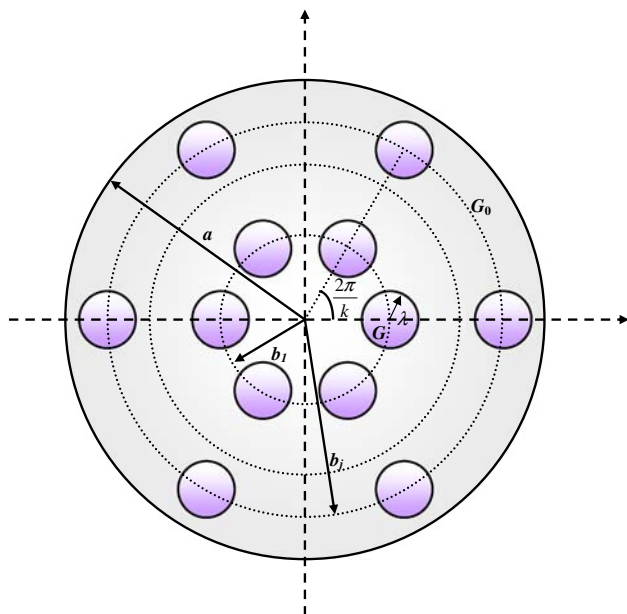


Fig. 9 A circular rod with several rings of circular inclusions

Table 6 Torsional rigidity of different cases for a circular bar with two and three rings of holes or inclusions

Case	$\frac{b_1}{a}$	$\frac{b_2}{a}$	$\frac{b_3}{a}$	$\frac{\lambda}{a}$	$\frac{G}{G_0}$	j	k	$\frac{G_{eff}}{G_0}$ [13]	$\frac{G_{eff}}{G_0}$ (present)
1	$\frac{3}{8}$	$\frac{3}{4}$	–	$\frac{1}{8}$	30	2	6	1.1205	1.3553
2	$\frac{1}{4}$	$\frac{17}{32}$	$\frac{13}{16}$	$\frac{3}{32}$	30	3	6	1.0618	1.2332
3	$\frac{3}{8}$	$\frac{3}{4}$	–	$\frac{1}{8}$	0	2	6	0.9636	0.7493
4	$\frac{1}{4}$	$\frac{17}{32}$	$\frac{13}{16}$	$\frac{3}{32}$	0	3	6	0.9745	0.7800

The geometry sketch is shown in Fig. 9. The results of our approach and those of Kuo and Conway are shown in Table 6. In a similar situation of the previous example, the torsional rigidities deviate with those of Kuo and Conway’s result. The reason may be explained in a similar way of Example 3.

Example 5 A circular rod with three circular inclusions.

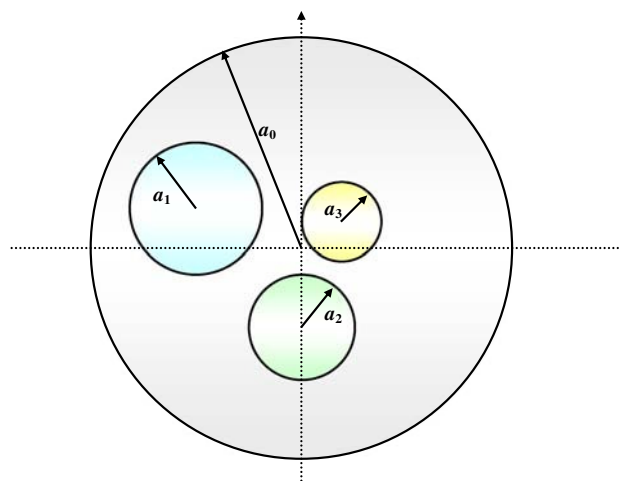


Fig. 10 A circular bar with three arbitrary circular inclusions

In this example, we design a circular rod with three arbitrary circular inclusions as shown in Fig. 10. The centers of three inclusions are $(-4, 1)$, $(0, 1.732)$ and $(0.75, 0.5)$. The radii of the circular bar and three inclusions are 0.4, 1.25, 1 and 0.5, respectively. The shear moduli are given as 1.0, 1.5, 2.25 and 0.5. For the case, the torsional rigidity is obtained as 1.11018 by using the present approach. The torsional rigidity of the circular holes is found to be 0.53209 by setting zero moduli of the three inclusions as a special case. The case shows the great generality of the present approach to deal with the problem of a torsion bar with arbitrary number, radii and position inclusions and/or holes.

5 Conclusions

Torsion problems with circular inclusions as well as holes have been successfully solved by using the present formulation. Here, we presented a different way to avoid the singular and hypersingular integrals by kernel separation instead of conventional bump contour approach. Our solutions match well with the exact solution if available and other solutions by using the integral formulation. Only 41 collocation points uniformly distributed on each boundary are required to obtain the accurate results of torsional rigidity with error less than 1% after comparing with the exact solution. For the stress response, our approach also agrees well with the analytical solution. The program was developed to deal with arbitrary number, different positions, various radii and shear moduli of inclusions. The proposed approach is free from calculating principal value, of boundary-layer effect, while the exponential convergence and the meshless method are included in the original elements and advantages of the method. Besides, the BIEs for the domain point or the null-field equation in our formulation can both be employed by exactly collocating the

538 point on the real boundary thanks to the introduction of the
539 degenerate kernels.

540 References

- 541 1. Ang WT, Kang I (2000) A complex variable boundary element
542 method for elliptic partial differential equations in a multiply-con-
543 nected region. *Int J Comput Math* 75:515–525
- 544 2. Bird MD, Steele CR (1991) Separated solution procedure for bend-
545 ing of circular plates with circular holes. *J Appl Mech* 59:398–404
- 546 3. Caulk DA (1983) Analysis of elastic torsion in a bar with circular
547 holes by a special boundary integral method. *J Appl Mech* 50:101–
548 108
- 549 4. Chen JT, Chen PY (2007) A semi-analytical approach for stress
550 concentration of cantilever beams with holes under bending.
551 *J Mech* 23(3):211–221
- 552 5. Chen JT, Chiu YP (2002) On the pseudo-differential operators in
553 the dual boundary integral equations using degenerate kernels and
554 circulants. *Eng Anal Bound Elem* 26:41–53
- 555 6. Chen JT, Hong H-K (1999) Review of dual boundary element
556 methods with emphasis on hypersingular integrals and divergent
557 series. *Appl Mech Rev* 52:17–33
- 558 7. Chen JT, Shen WC, Chen PY (2006) Analysis of circular torsion
559 bar with circular holes using null-field approach. *CMES* 12:109–
560 119
- 561 8. Chen T, Weng IS (2001) Torsion of a circular compound bar with
562 imperfect interface. *J Appl Mech* 68:955–958
- 563 9. Crouch SL, Mogilevskaya SG (2003) On the use of Somigliana's
564 formula and Fourier series for elasticity problems with circular
565 boundaries. *Int J Numer Methods Eng* 58:537–578
- 566 10. Jin B (2004) A meshless method for the Laplace and biharmonic
567 equations subjected to noisy boundary data. *CMES* 6:253–262
- 568 11. Katsikadelis JT, Sapountzakis EJ (1985) Torsion of composite bars
569 by boundary element method. *J Eng Mech* 111:1197–1210
- 570 12. Kuo YM, Conway HD (1973) The torsion of composite tubes and
571 cylinders. *Int J Solids Struct* 9:1553–1565
- 572 13. Kuo YM, Conway HD (1974) Torsion of cylinders with multiple
573 reinforcement. *J Eng Mech Div* 100:221–233
14. Ling CB (1947) Torsion of a circular tube with longitudinal
574 circular holes. *Q Appl Math* 5:168–181 575
15. Lurje AI (1970) *Theory of elasticity*. Nauka Publisher, Moscow
576 (in Russian) 577
16. Mogilevskaya SG, Crouch SL (2001) A Galerkin boundary inte-
578 gral method for multiple circular elastic inclusions. *Int J Numer*
579 *Methods Eng* 52:1069–1106 580
17. Morse PM, Feshbach H (1978) *Methods of theoretical physics*.
581 McGraw-Hill, New York 582
18. Murakami H, Yamakawa J (1998) Torsional wave propagation in
583 reinforced concrete columns. *Int J Solids Struct* 35:2617–2637 584
19. Muskhelishvili NI (1963) *Some basic problems of the mathemat-
585 ical theory of elasticity*. P. Noordhoff, Groningen 586
20. Naghdi AK (1991) Bending of a perforated circular cylindrical
587 cantilever. *Int J Solids Struct* 28(6):739–749 588
21. Petrov EP (1997) Analysis of torsion and shear characteristics of
589 beam cross-sections by the boundary element method. *Int J BEM*
590 *Commun* 8:239–245 591
22. Sapountzakis EJ, Mokos VG (2001) Nonuniform torsion of com-
592 posite bars by boundary element method. *J Eng Mech, ASCE*
593 127(9):945–953 594
23. Sapountzakis EJ, Mokos VG (2003) Warping shear stresses in non-
595 uniform torsion of composite bars by BEM. *Comput Methods Appl*
596 *Mech Eng* 192:4337–4353 597
24. Sapountzakis EJ, Mokos VG (2004) Nonuniform torsion of com-
598 posite bars of variable thickness by BEM. *Int J Solids Struct*
599 41(7):1753–1771 600
25. Shams-Ahmadi M, Chou SI (1997) Complex variable boundary
601 element method for torsion of composite shafts. *Int J Numer*
602 *Methods Eng* 40:1165–1179 603
26. Sladek V, Sladek J, Tanaka M (2005) Local integral equations and
604 two meshless polynomial interpolations with application to poten-
605 tial problems in non-homogeneous media. *CMES* 7:69–84 606
27. Tang RJ (1996) *Torsion theory of the crack cylinder*. Shanghai Jiao
607 Tong University Publisher, Shanghai (in Chinese) 608
28. Timoshenko SP, Goodier JN (1970) *Theory of elasticity*. McGraw-
609 Hill, New York 610